Supplementary Information for

Direct electrochemical generation of supercooled sulfur microdroplets well below their melting temperature

Nian Liu[1,2,3,†,*], Guangmin Zhou[2,†], Ankun Yang[2], Xiaoyun Yu[2], Feifei Shi[2], Jie Sun[2], Jinsong Zhang[2], Bofei Liu[2], Chun-Lan Wu[2], Xinyong Tao[2,4], Yongming Sun[2], and Yi Cui[2,5,*], Steven Chu[1,6,*]

[1] Department of Physics, Stanford University, Stanford, California 94305, USA.

[2] Department of Materials Science and Engineering, Stanford University, Stanford, California 94305, USA.

[3] School of Chemical & Biomolecular Engineering, Georgia Institute of Technology, Atlanta, GA 30332, USA.

[4] College of Materials Science and Engineering, Zhejiang University of Technology, Hangzhou 310014, China.

[5] Stanford Institute for Materials and Energy Sciences, SLAC National Accelerator Laboratory, 2575 Sand Hill Road, Menlo Park, CA 94025, USA.

[6] Department of Molecular and Cellular Physiology, Stanford University, Stanford, California 94305, USA.

[†] These authors contributed equally.

Correspondence and requests for materials should be addressed to N.L. (*email: nian.liu@chbe.gatech.edu), Y.C. (*email: yicui@stanford.edu) or S.C. (*email: schu@stanford.edu).

www.pnas.org/cgi/doi/10.1073/pnas.1817286115

Supplementary Figures

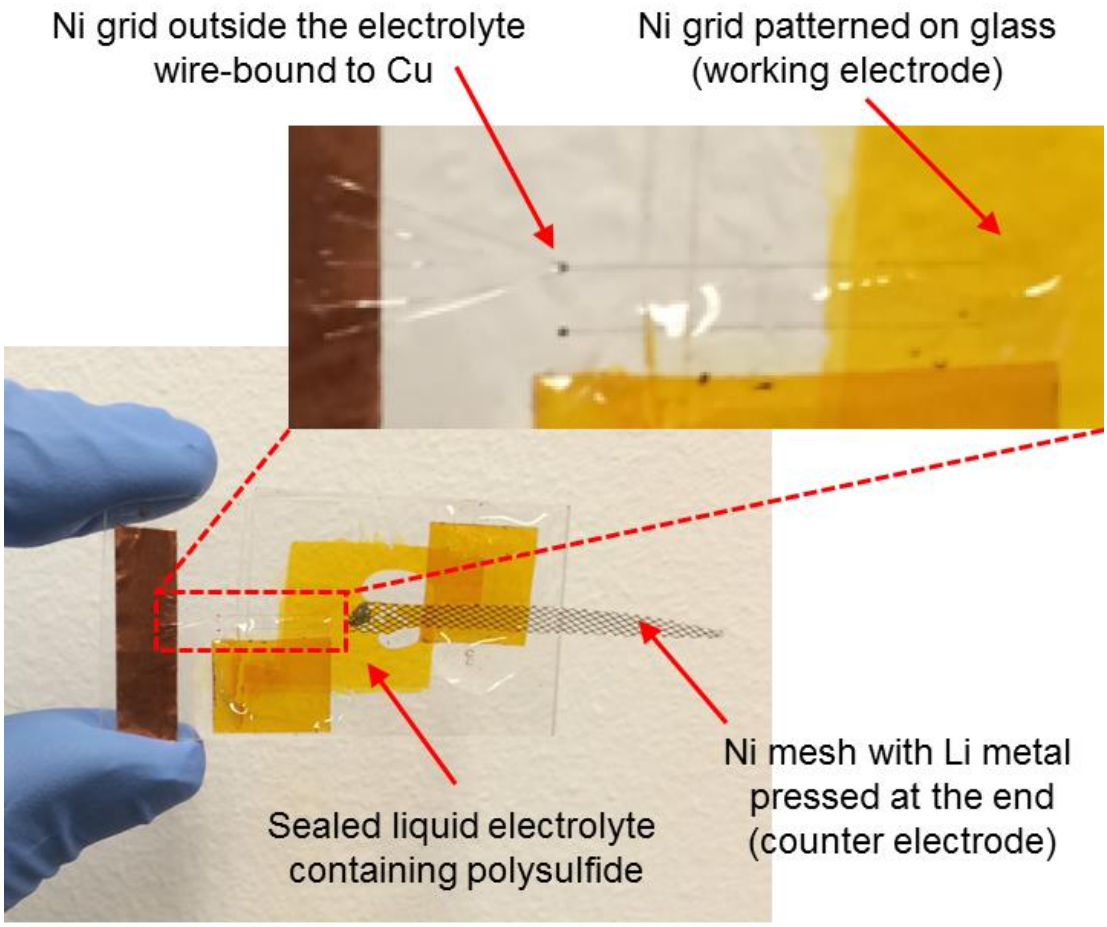

Fig. S1. Pictures of an electrochemical cell developed for *in-operando* light microscopy of sulfur electrochemistry.

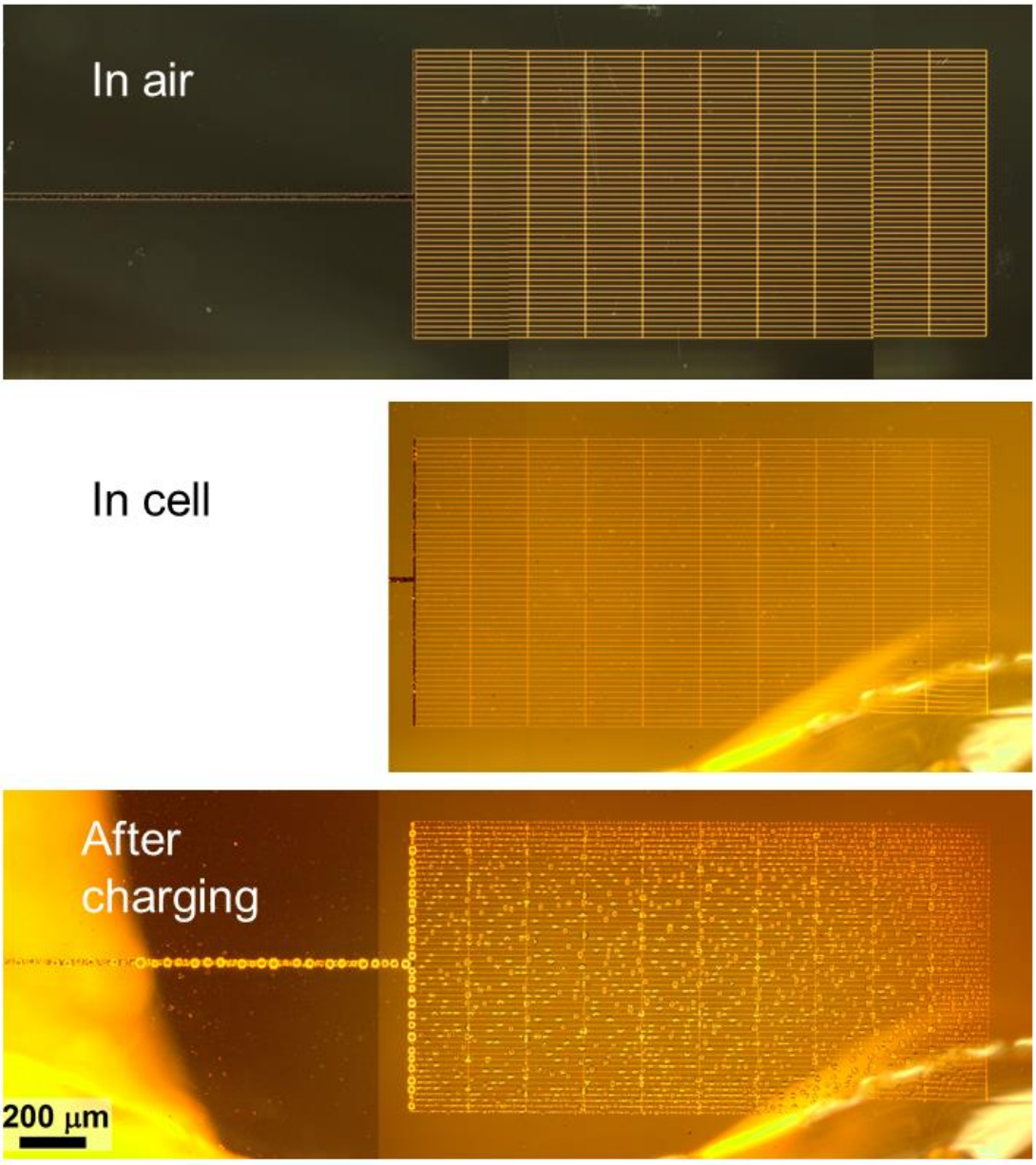

Fig. S2. Optical microscopy image of the Ni grid on glass as fabricated, after cell assembly, and after electrochemical charging. After charging, super-cooled sulfur droplets can be found everywhere on the Ni grid.

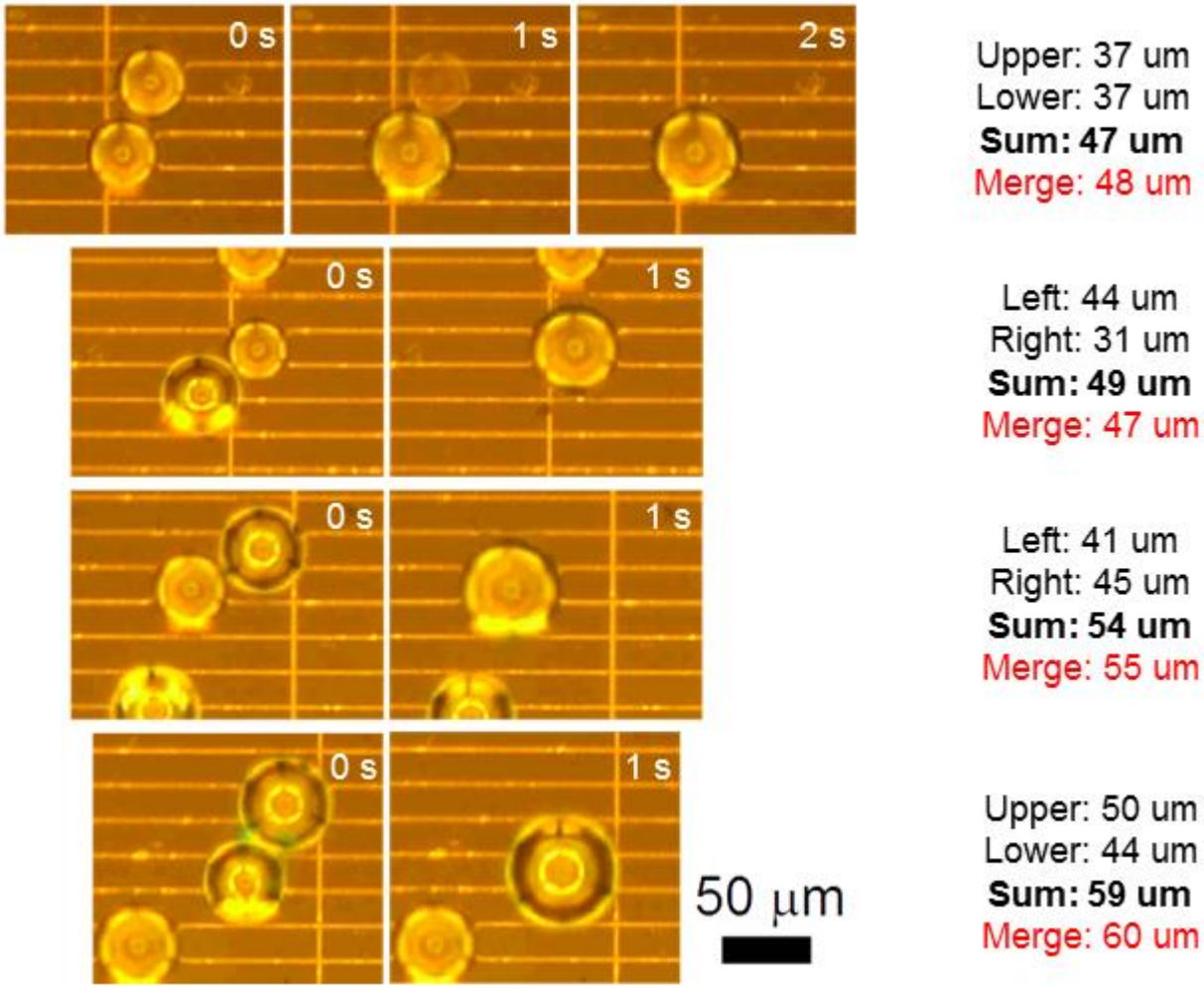

Fig. S3. Four sets of time-lapse images showing rapid merging of neighboring droplets and relaxation to spherical shape within one second, at room temperature, indicating the liquid nature of sulfur. The diameters of droplets before and after merging are shown on the right. "Sum" is the calculated diameter of the merged droplet assuming simple addition of volume and spherical shape, "Merge" is the measured diameter, which agrees well with "Sum".

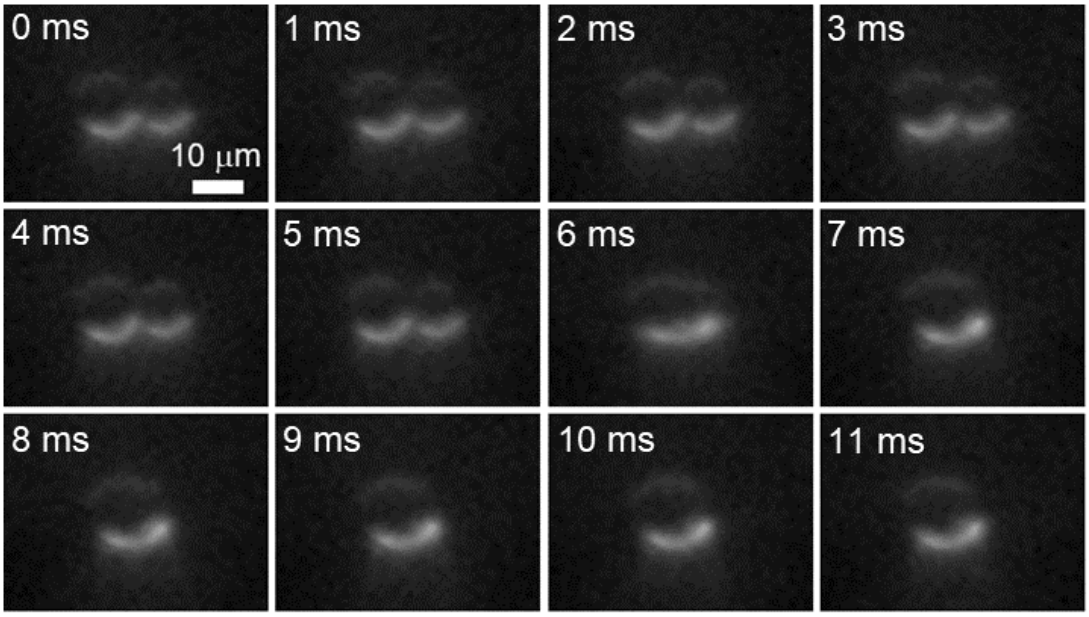

Fig. S4. Time-lapse images (1 ms interval) of a super-cooled liquid sulfur droplet merging event recorded using high speed camera (Phantom v1210) mounted on a Nikon inverted scope with 40x air objective.

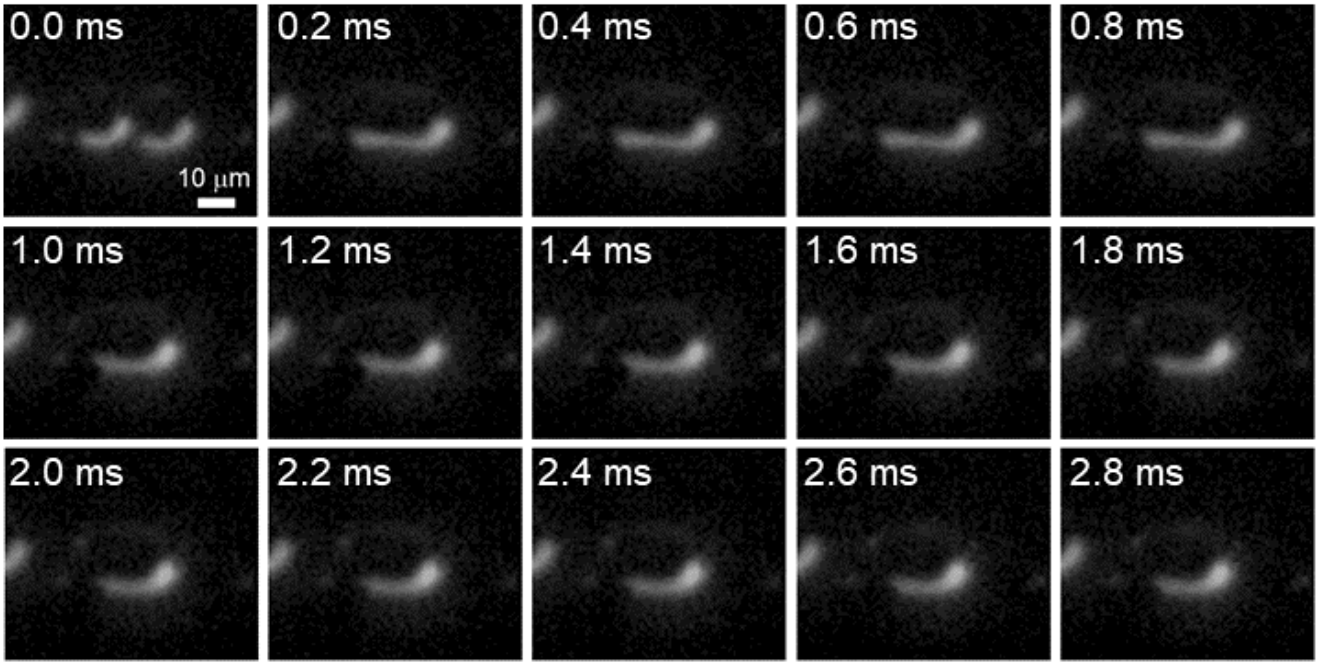

Fig. S5. Time-lapse images (0.2 ms interval) of a super-cooled liquid sulfur droplet merging event recorded using high speed camera (Phantom v1210) mounted on a Nikon inverted scope with 40x air objective.

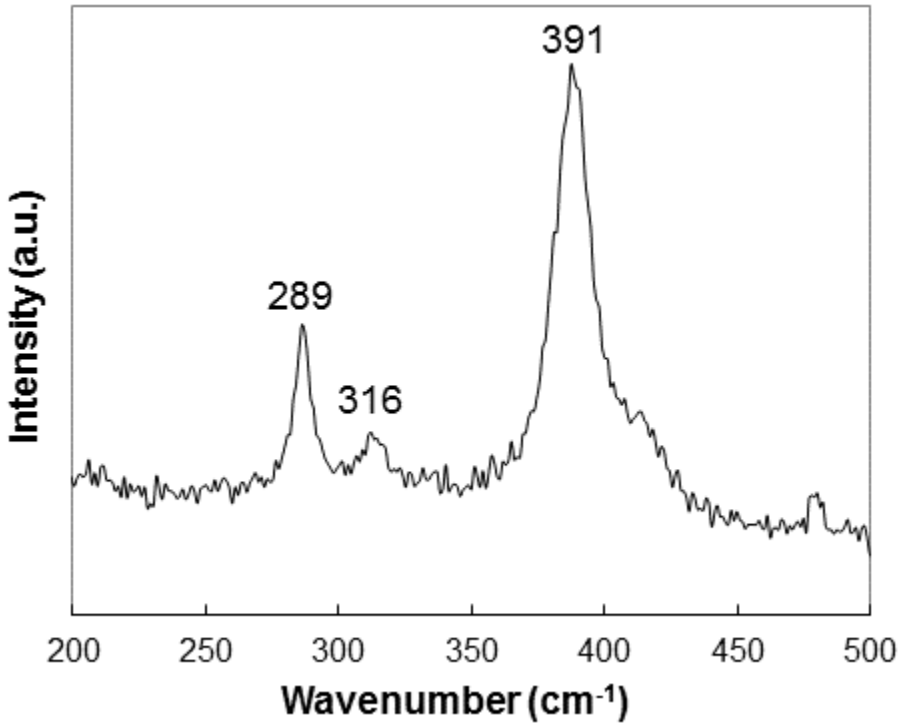

Fig. S6. Raman spectrum of fabricated CoS_2 film on glass. CoS_2 were coated on glass via Co evaporation (100 nm) and subsequent sulfurization (1).

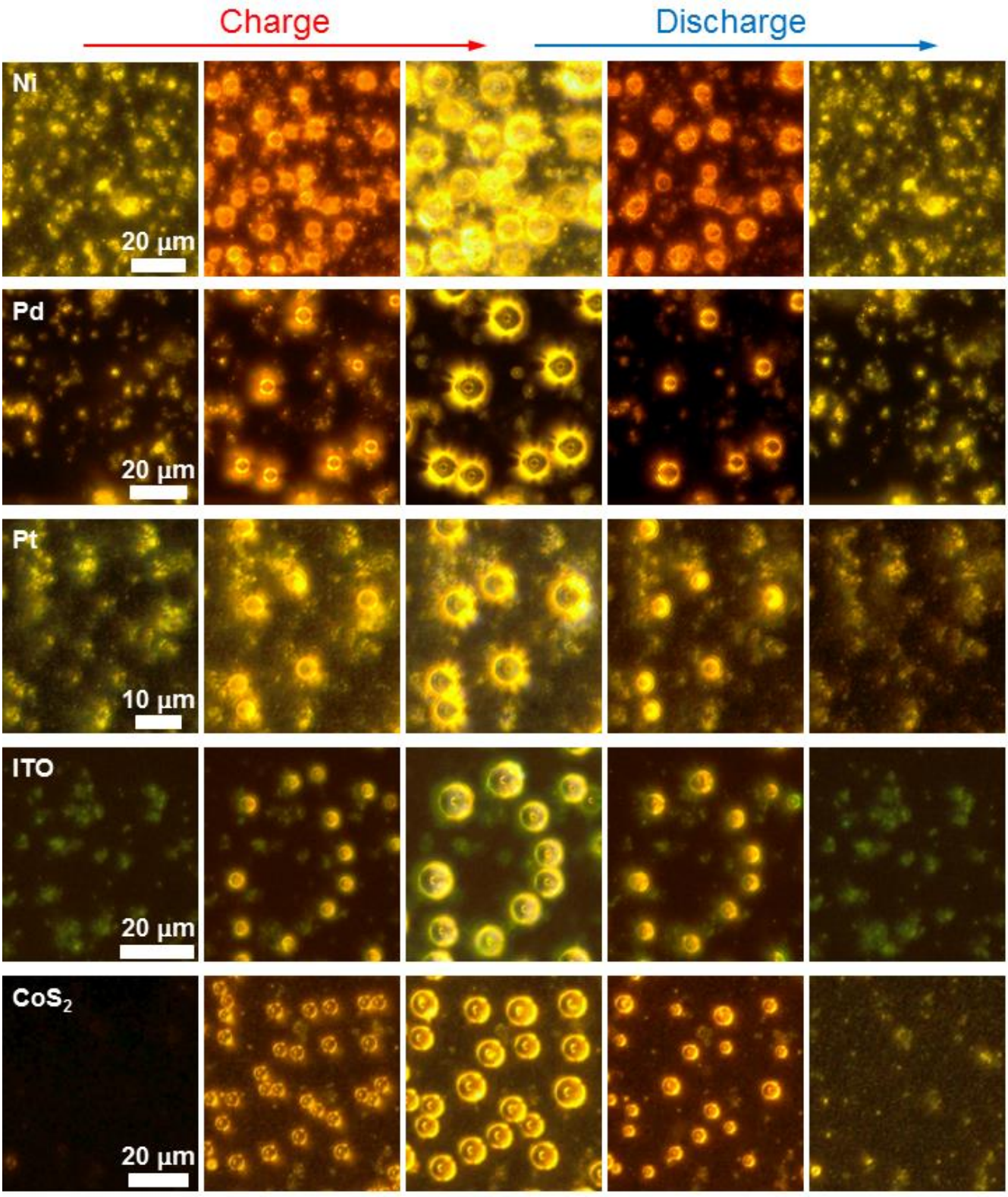

Fig. S7. Time-lapse images of the formation of super-cooled sulfur droplets on various substrates. Full movies are found in Movies S3-S7. Ni film (50 nm) was coated on glass slide using thermal evaporator; Pd and Pt films (50 nm in both cases) were coated on glass using e-beam evaporator, ITO film (200 nm) were coated on glass via sputtering.

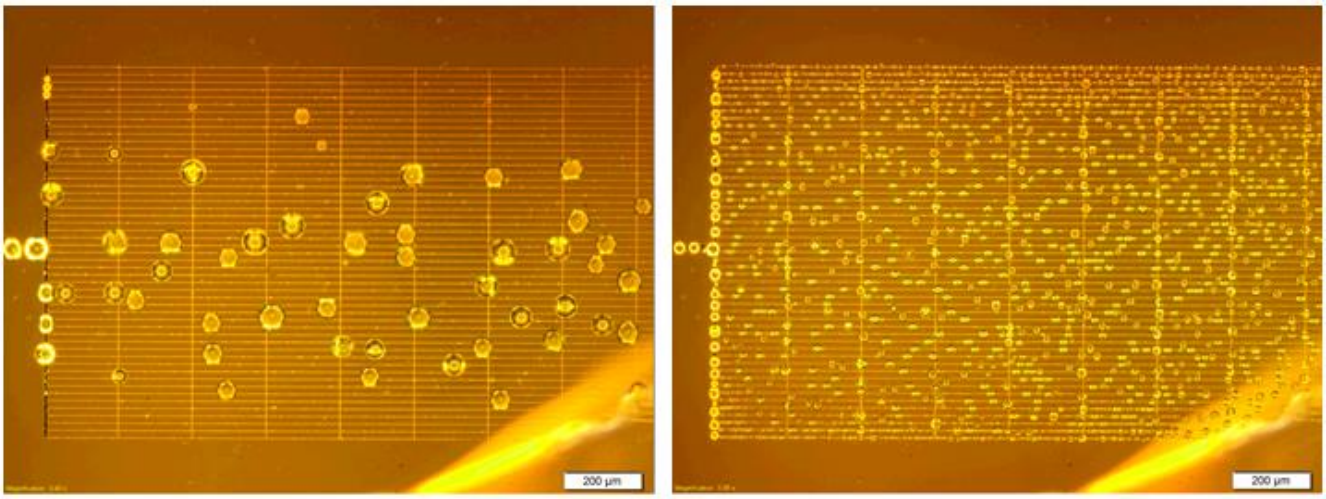

Fig. S8. Large sulfur droplets formed with low current and long duration (0.01 mA, 60 min, left image), and small sulfur droplets formed with high current and short duration (0.05 mA, 6 min, right image).

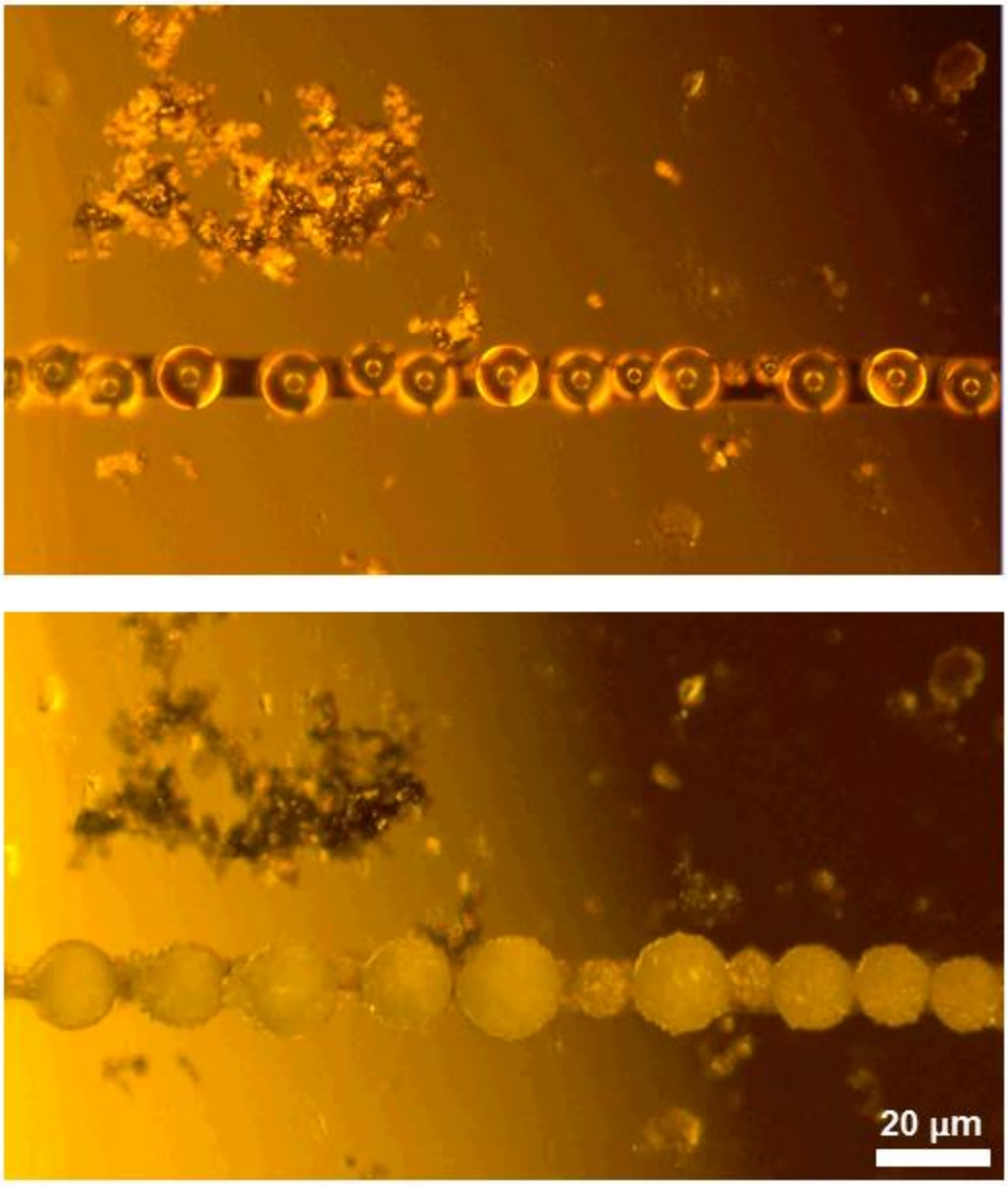

Fig. S9. As formed super-cooled sulfur droplets (upper image) and after solidification upon touched by crystalline sulfur (lower image).

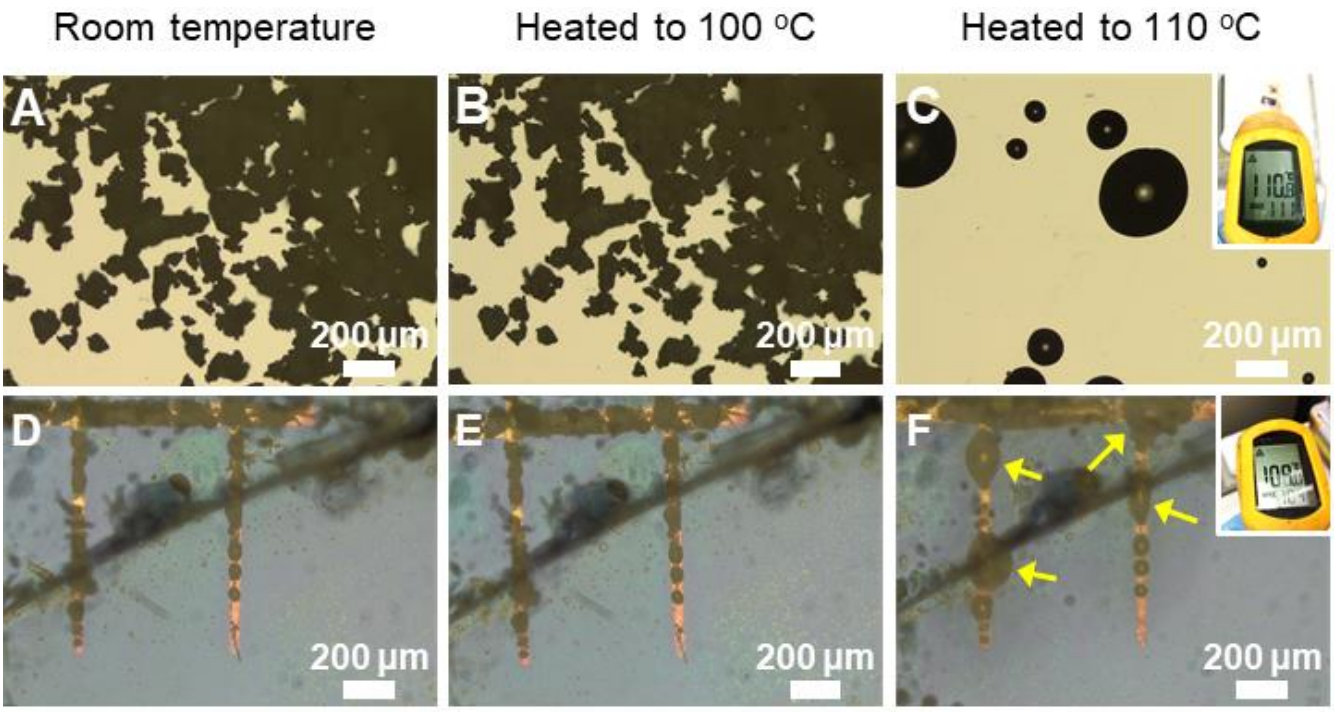

Fig. S10. In situ heating of S_8 powders (*A*-*C*) and electrochemically generated liquid sulfur droplets after being solidified (*D*-*F*). Insets of (*C*) and (*F*) show the measurement of temperature using infrared thermometer. Neither sample melt at 100 °C, both melt at 110 °C. The melting point of solidified electrochemically generated liquid sulfur droplets is close to pure S_8 powders, indicating that the sulfur droplets are not likely highly doped with other species.

A

Cooling bath mixtures		
Cooling agent	Organic solvent or salt	Temp (°C)
Ice	Salts	0 to −40
Dry ice	o-Xylene	−29
Dry ice	EtOH	−72

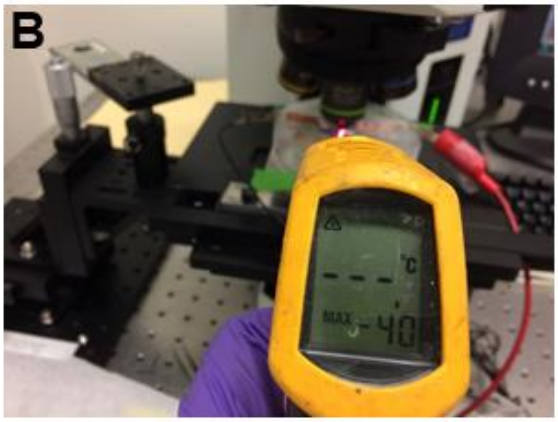

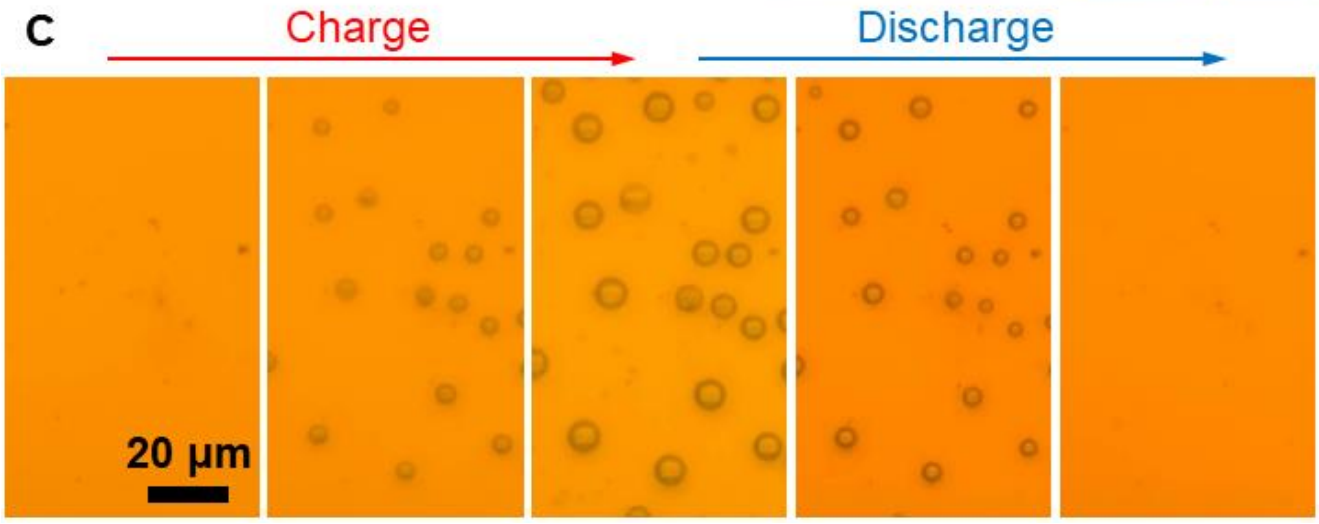

Fig. S11. Direct electrochemical generation of super-cooled sulfur droplets at < −40 °C. (*A*) Temperature of various mixture cooling bath. (*B*) Picture of a sulfur electrochemical cell in dry ice and ethanol mixture cooling bath. The temperature at the position of observation is lower than −40 ºC, the lower limit of measurement of the infrared thermometer. (*C*) Time-lapse light microscopy images of the electrochemical generation and consumption of sulfur droplets on Au electrode at < −40 °C. For the full video, see Movie S14.

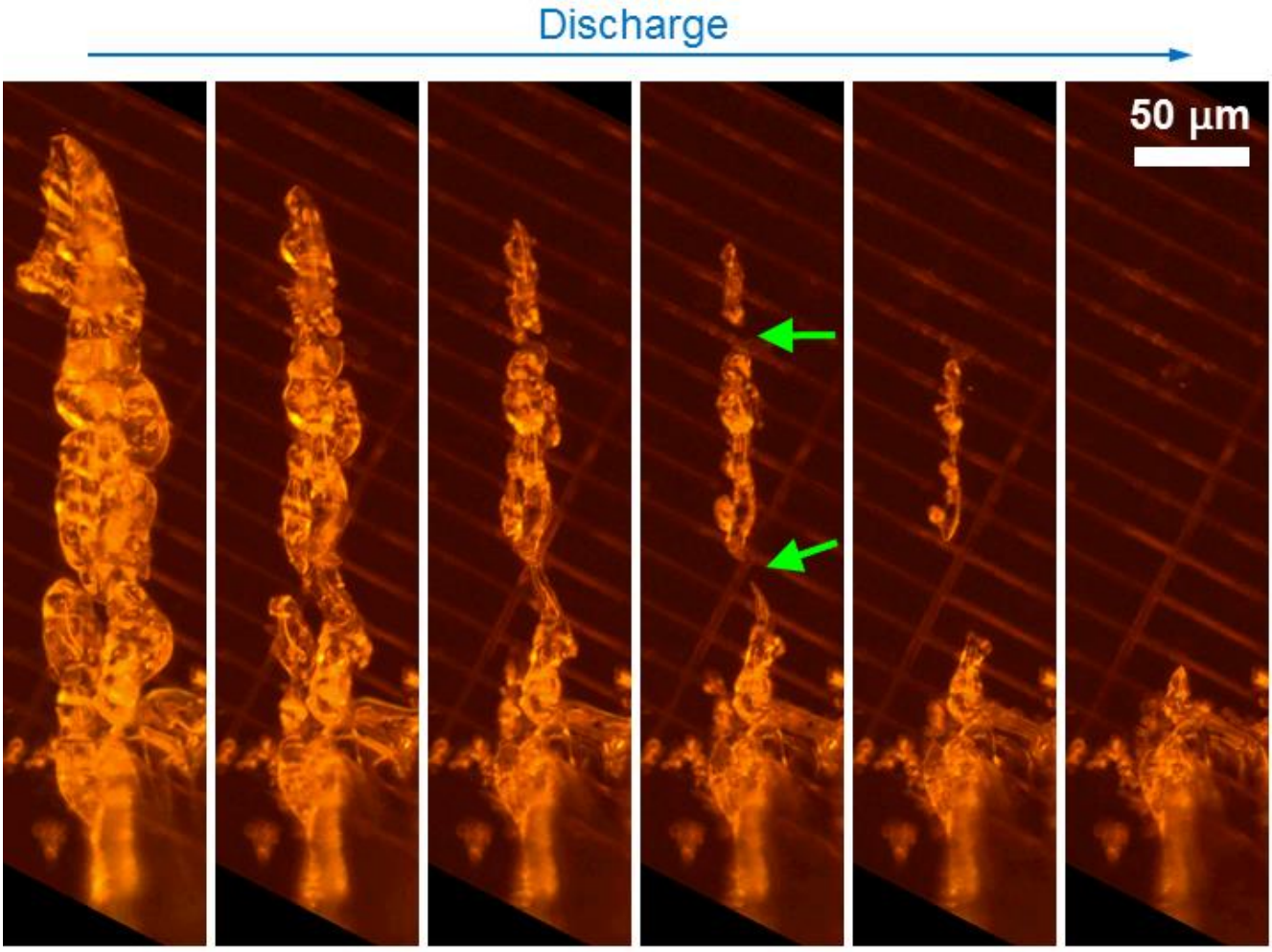

Fig. S12. Time-lapse images of a solid sulfur crystal upon electrochemical discharging. The green arrows indicate the disconnection of the needle-like crystal. Notice the metal grid at the background was off focus, indicating the crystal extended out of the plane of the metal grid. The reaction of the disconnected segments implies the existence of solution mechanism. For the full video, see Movie S15.

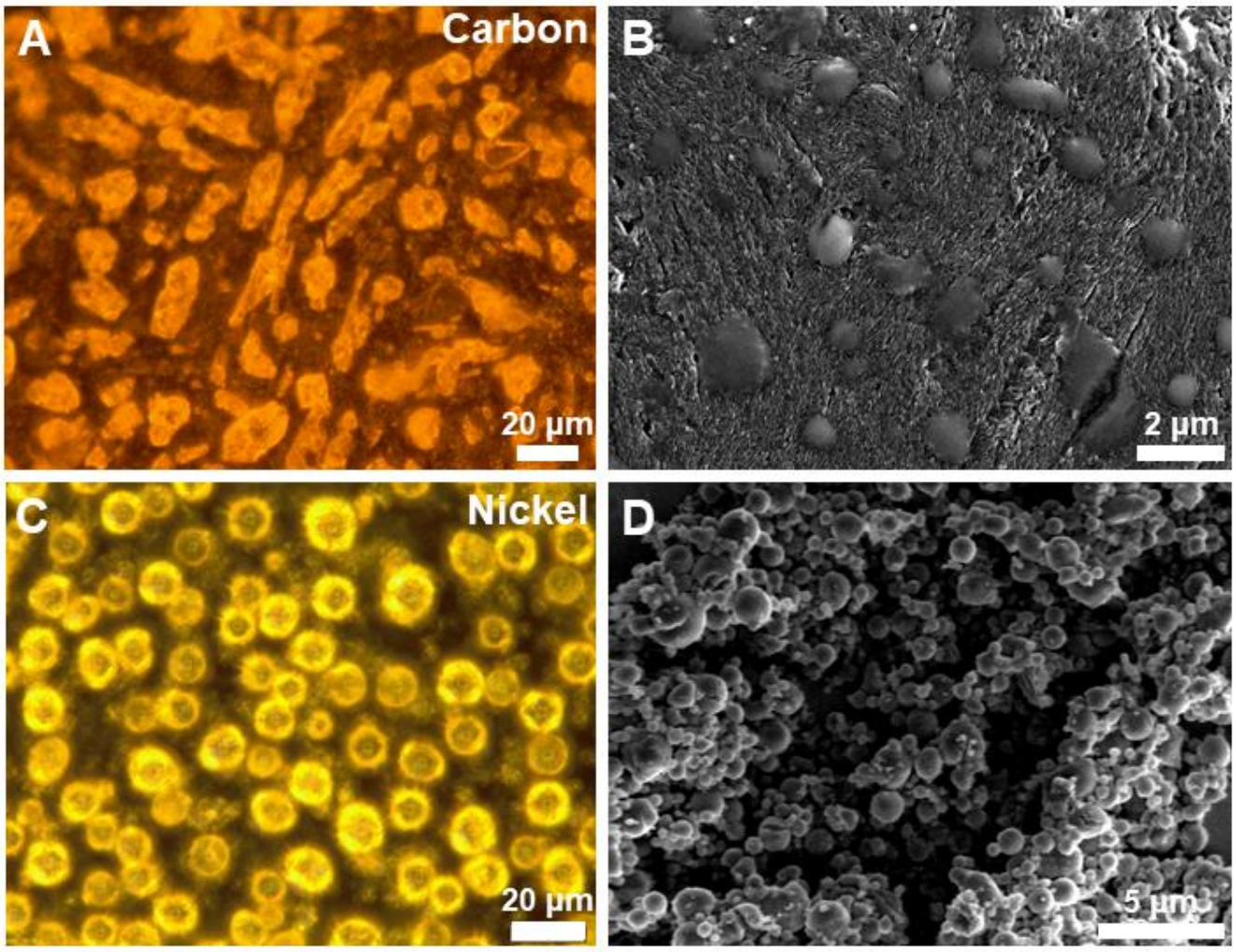

Fig. S13. (*A* and *B*) *In-operando* DFLM image (*A*) and *ex-situ* SEM image (*B*) of electrochemically deposited crystalline sulfur on carbon. (*C* and *D*) *In-operando* DFLM image (*C*) and *ex-situ* SEM image (*D*) of electrochemically deposited super-cooled sulfur droplets on Ni film. The mildness of light allows for in operando imaging in real electrolyte, and in real time, which captures the formation and merging of sulfur microdroplets on Ni substrate.

Supplementary Movies

Movie S1. Super-cooled liquid sulfur microdroplets formation on Ni lines patterned on glass. The electrochemical cell was discharged first, and then charged. Play speed is 32x of the actual speed. The yellow and dark red color of the electrolyte are from various polysulfide (S_8^{2-}, S_6^{2-}, S_4^{2-}, etc) (2).

Movie S2. Large-area view of the same process in Supplementary Movie S1, showing the uniform growth of super-cooled sulfur everywhere on the Ni pattern. Play speed is 32x of the actual speed.

Movie S3. Super-cooled liquid sulfur microdroplets formation on Ni thin film coated on glass. The electrochemical cell was charged first, and then discharged. Play speed is 32x of the actual speed.

Movie S4. Super-cooled liquid sulfur microdroplets formation on Pd thin film coated on glass. The electrochemical cell was charged first, and then discharged. Play speed is 32x of the actual speed.

Movie S5. Super-cooled liquid sulfur microdroplets formation on Pt thin film coated on glass. The electrochemical cell was charged first, and then discharged. Play speed is 32x of the actual speed.

Movie S6. Super-cooled liquid sulfur microdroplets formation on ITO thin film coated on glass. The electrochemical cell was charged first, and then discharged. Play speed is 64x of the actual speed.

Movie S7. Super-cooled liquid sulfur microdroplets formation on CoS_2 thin film coated on glass. The electrochemical cell was charged first, and then discharged. Play speed is 64x of the actual speed.

Movie S8. Solid sulfur crystals formation on glassy carbon. The electrochemical cell was charged first, and then discharged. Play speed is 64x of the actual speed.

Movie S9. Co-existing liquid sulfur and solid sulfur formation in one cell, as a result of co-existing Ni and graphite nanoplatelets. The electrochemical cell was being charged. Play speed is 64x of the actual speed. The co-existence of solid sulfur also proves that the temperature inside the cell is below sulfur's melting point.

Movie S10. Instantaneous solidification of a super-cooled sulfur microdroplet initiated by the touch of a growing sulfur crystal. The electrochemical cell was being charged. Play speed is 4x of the actual speed.

Movie S11. Instantaneous solidification of a chain of super-cooled sulfur microdroplets initiated by the touch of a growing sulfur crystal. The electrochemical cell was being charged. Play speed is 16x of the actual speed.

Movie S12. Super-cooled liquid sulfur microdroplets generation and dissolution on Au thin film coated on glass. The electrochemical cell was kept at −28.4 °C (in dry ice and o-Xylene mixture bath) while being charged and discharged. Play speed is 5x of the actual speed.

Movie S13. The same electrochemical cell shown in Supplementary Movie S12 was warmed to room temperature and then charged and discharged. Play speed is 10x of the actual speed.

Movie S14. Super-cooled liquid sulfur microdroplets generation and dissolution on Au thin film coated on glass. The electrochemical cell was kept below −40 °C (in dry ice and ethanol mixture bath) while being charged and discharged. Play speed is 2x of the actual speed.

Movie S15. Electrochemical reduction of a solid sulfur crystal to polysulfide. The electrochemical cell was being discharged. Play speed is 16x of the actual speed. The sulfur crystal grew from a graphite nanoplatelet sitting on the Ni grid. The background Ni grid was far off focus, indicating the rod-shaped crystal inclined up instead of lay on the Ni grid.

Movie S16. Electrochemical reduction of solid sulfur crystals to polysulfide. The electrochemical cell was being discharged. Play speed is 10x of the actual speed.

References

1. Kong D, Cha JJ, Wang H, Lee HR, Cui Y (2013) First-row transition metal dichalcogenide catalysts for hydrogen evolution reaction. *Energy Environ Sci* 6(12):3553.
2. Sun Y, et al. (2015) In-operando optical imaging of temporal and spatial distribution of polysulfides in lithium-sulfur batteries. *Nano Energy* 11:579–586.